Available online at www.sciencedirect.com
SCIENCE DIRECT®
International Journal of Solids and Structures 42 (2005) 5887–5904
INTERNATIONAL JOURNAL OF SOLIDS and STRUCTURES
www.elsevier.com/locate/ijsolstr

Force on inner hair cell cilia

Charles R. Steele [a,*], Sunil Puria [a,b,1]

[a] Stanford University, Durand Building, Room 262, Stanford, CA 94305, USA
[b] Department of Otolaryngology-Head and Neck Surgery, Stanford University, Stanford, CA 94305, USA

Received 7 January 2005
Available online 26 May 2005

Abstract

The cochlea of the inner ear transforms the incoming sound pressure into neural excitation. Despite extensive experiments and modeling for the past century, understanding the behavior of the cochlea is far from complete. With an efficient program (Fast4) for shell of revolution structures, all mechanical (elastic) details of the curved cochlear cross-section and the organ of Corti can be computed. Based on the known values for the elastic moduli of the protein fibers and estimates for the geometry, the responses to point and pressure loads have been calculated which are reasonably close to the direct measurements. In the present work, the details of the inner hair cell are included, with a fluid gap between the tip of the cilia and the Hensen stripe of the tectorial membrane. A simple model for the near contact indicates nonlinear response similar to the intracellular recordings. This near contact is included into a more complete elastic model for the organ of Corti that includes three rows of cilia and tip links. The phase of the maximum tension of the tip link, which causes excitation of the cell, is computed for low frequencies for comparison to measurements. For low frequencies the fluid motion in the organ of Corti is approximately two-dimensional. The phase is found to be affected by: (1) geometrical difference between basal and upper turns of the cochlea, (2) initial gap spacing between the tip of the cilium and the Hensen stripe, (3) initial gap spacing between the tip of the cilium and the tectorial membrane, (4) presence of an electrode probe constraint on the motion of the inner hair cell, and (5) the stiffness of the tectorial membrane. The latter is the most significant. For a soft tectorial membrane, the excitation is generally between maximum velocity and displacement of the basilar membrane toward scala vestibuli. However, for a stiff tectorial membrane, the phase changes to an excitation with velocity and displacement toward scala tympani. Thus a possible mechanical reason is offered for the auditory nerve excitation in the base of the chinchilla cochlea for basilar membrane velocity toward scala tympani and in the middle and upper turns of the guinea pig cochlea, excitation for velocity toward scala vestibuli.

Keywords: Cochlea; Mechanical response; Cilia; Organ of Corti; Hensen stripe; Inner hair cell; Tectorial membrane

* Corresponding author. Tel.: +1 650 723 2844; fax: +1 650 723 1778.
E-mail addresses: chasst@stanford.edu (C.R. Steele), puria@stanford.edu (S. Puria).
[1] Tel.: +1 650 723 8089.

0020-7683/$ - see front matter © 2005 Elsevier Ltd. All rights reserved.
doi:10.1016/j.ijsolstr.2005.03.056

1. Introduction

Progress toward understanding the function of the cochlea of the inner ear has continued at a rapid rate with improved quality and variety of measurement procedures. This study is motivated by the measurements of the inner hair cell (IHC) response by Cheatham and Dallos (1999) in the upper turns of the guinea pig cochlea and the eighth nerve and basilar membrane (BM) responses in the base of the chinchilla by Ruggero et al. (2000). For low frequencies, the phase of IHC and eighth nerve responses are synchronized with the BM. The IHC at the apex behaves as might be expected, with a maximum excitation when the BM is between maximum displacement and velocity toward scala vestibuli (SV). However, the neural recordings at the base indicate excitation with velocity toward scala tympani (ST). The objective of this work is to determine whether or not such behavior is indicated from the computation of a fairly accurate model of the organ of Corti (OC). For this the details of the flow on the cilia of the inner hair cell are considered, which may be similar to flow in other organs such as that studied by Weinbaum et al. (2001).

For all the elaborate detail of the OC, it is interesting that the neural response mirrors the motion of the BM, as shown by Narayan et al. (1998). So the OC does not serve as a "second filter" to improve the tuning of the BM, but interacts directly with the BM. However, the passive response of the cochlea can be explained rather well by stripping off the OC. Our computation for this is based on a standard WKB asymptotic wave analysis method. Steele and Taber (1979) confirm that this procedure is accurate in computing models with three-dimensional (3-D) viscous fluid when all the geometric and physical properties are known in an experimental model. The direct numerical integration of the 3-D viscous equations by Givelberg and Bunn (2003) shows promise, but requires considerable computing time, hours on a high-speed parallel computer (compared to seconds for WKB on a desktop computer for a given frequency). Their "complete" cochlear model does not include the organ of Corti (OC).

The OC obviously adds an important active sharpening of the response. Various models for this use an active mechanical system added to the BM. For most, the model parameters are difficult to relate to the physical features of the OC. However, a physically based, cochlear model consisting of a basilar membrane with a simplified representation of the OC in a three-dimensional fluid (3-D), using a WKB-numerical approximation, simulates the passive, active, transient and nonlinear behavior surprisingly well (Lim and Steele, 2003).

Nevertheless, the elaborate details of the OC exist for a reason, namely to deliver the correct fluid forces against the cilia of the inner hair cell (IHC). Several laboratories are improving the computation for the cochlea with the OC. Kolston (1999) presents an extensive 3-D finite element model with the OC approximated with rectangular frames and inviscid fluid. Bohnke and Arnold (1998) model the actual anatomy, but only in a restricted region. Cai and Chadwick (2002) use a finite element solution for the cross-section of the OC treated as a continuous medium, combined with WKB for the longitudinal waves, and Andoh and Wada (2003) include the details of the cilia of the outer hair cells (OHC).

We are using an alternate approach with a computer program (Fast4) developed for the computation of axisymmetric shell structures. This uses a combination of asymptotic and direct numerical methods (Steele and Shad, 1995), that is efficient in comparison with standard finite element methods and requires minimal input. Specifically, the mesh required is generated in the program. With this program most of the mechanical detail of the OC can be included. Preliminary work has begun (Steele, 1999) on an efficient procedure for handling both the fluid waves and the detailed OC for the high frequency response.

The present work is apparently the first to model the mechanical environment of the cilia of the inner hair cell (IHC) in a full OC and fluid environment. Preliminary results are given by Steele and Puria (2003). Since the phase locking of the neural response occurs only for low frequency, this provides an excellent motivation to get the geometry, stiffness, and viscous fluid treated properly, with a 2-D treatment of the cross-section and without the concern for the one or more modes of longitudinal traveling waves that are certainly significant for higher frequencies.

2. Methods

2.1. Geometry

Such basic features of BM length, width distribution, and transverse fiber density are reasonably well established. This study, however, requires much more detail of the anatomy of the OC. Kelly (1989) provides such detail for the cross-section at the apex of the GP cochlea, about 17 mm from the stapes, averaged over a number of animals. His values for the geometry are used in our model for the apical section shown in Fig. 1, in which some of the important components of the structure are labeled. Other components are defined in the caption of Fig. 1.

This detail is not available for other locations. Consequently, the specific dimensions for the cross-section near the base of the cochlea, say at 3.5 mm from the stapes, are taken from a micrograph by Dunnebier et al. (1998). The model representation is shown in Fig. 2. In addition, Ulfendahl and colleagues (personal communication) have furnished micrographs of the entire GP cochlea. Zetes et al. (2004) summarize details of the fiber density and lengths for the hair cells, pillar cells, Deiter rods, and phalangeal processes at different locations in the GP.

The unfixed preparation of the gerbil cochlea used by Edge et al. (1998) is particularly important. This indicates that the Hensen stripe (HS) on the lower surface of the TM is close to the tips of the IHC cilia. Because of the shrinkage of the TM in the usual preparation, this stripe is normally seen at some distance from the IHC cilia. A closer view of the cilia of the IHC in the model is in Fig. 3. The three rows of cilia and the tip links are included. The dashed lines show the unloaded position, with the tip of the tallest cilia near the intersection of the Hensen stripe and the TM. The exact location of the stripe remains under investigation at different laboratories, so different initial gaps are considered in the present study. The tips of the

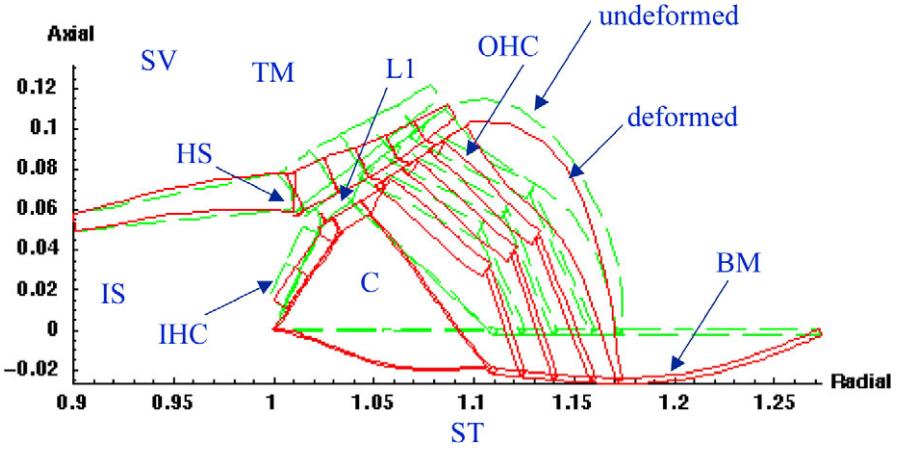

Fig. 1. Elastic Fast4 shell model for organ of Corti in apical turn of guinea pig. The loading is static pressure on the basilar membrane with no effect of the fluid. The dashed and solid lines show the undeformed and deformed configurations, respectively. The labels are for the tectorial membrane TM, outer hair cells OHC, basilar membrane BM, inner hair cells IHC, and Hensen strip HS. The fluid regions are scala vestibuli SV, the region under the tectorial membrane L_1, the scala tympani ST, and the inner sulcus IS. The additional fluid region is the Cortilymph (C) located in the inner tunnel region. Not labeled are the following components. The bottom of the triangular region C is the arcuate zone of the BM, the left side is the inner pillars (IP) and the right side the outer pillars (OP) of the arches of Corti. The Cortilymph extends through the spaces between the OP and surrounds the OHC. The membrane in which the upper end of the OHC, IHC and pillar head is embedded is the recticular lamina (RL). On the right of the OHC are the Hensen cells. The fluid bounded by the TM and RL, between the first and second OHC is L_2, and that between the second and third OHC is L_3. The Deiter rods are the links between the lower ends of the OHC and the BM. The radial distance is from the axis of the cochlea, and the axial distance is from the plane of the BM, both in millimeters.

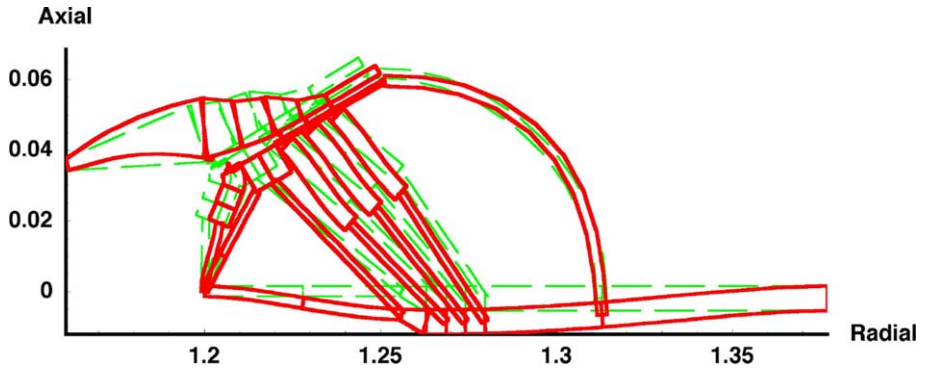

Fig. 2. Elastic Fast4 shell model for organ of Corti in basal turn of guinea pig. The dashed lines show the unloaded and the solid lines the deformed configuration due to a static pressure in SV. The radial and axial distances are in millimeters.

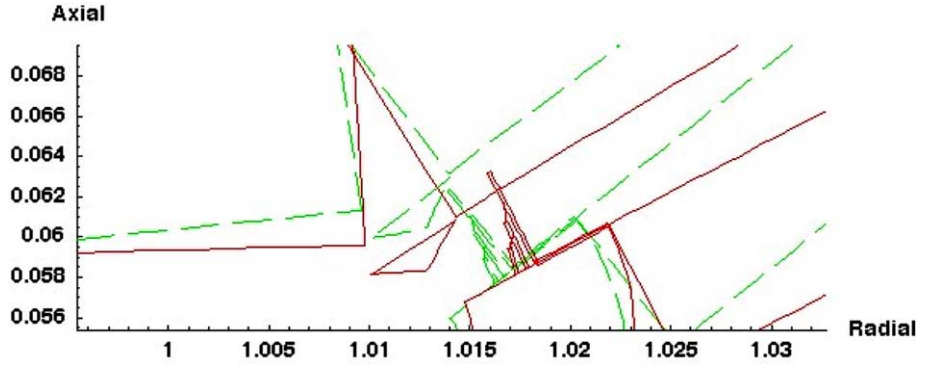

Fig. 3. Close-up view of inner hair cell (IHC) cilia and Hensen stripe (HS). The cross-section of the model Hensen stripe is the triangle that appears to be floating, but is actually attached to the TM located above. The three rows of cilia and the tip links are included in the calculation. The amplitude of displacement is greatly exaggerated, which makes it appear that the tall cilium penetrates the TM.

tallest IHC are not attached to the overlying TM. However, there exist filaments that connect the top of the IHC to the TM that have not been included in the present study. We presume that these do not affect the fluid flow near the tips of the cilia.

2.2. Elasticity

The objective is to use stiffness values for the components of the OC that are consistent with the microstructure and with direct stiffness measurements. The following summarizes the current assumptions.

1. Each component is a shell of revolution (Figs. 1 and 2) for which the linear elastic response is efficiently calculated with the Fast4 program. This program has been subjected to extensive validation with closed form solutions and finite element solutions over the past 15 years. The input for the cochlea is a file with the parameters of the cochlear cross-section at various distances from the stapes, as described in some detail in Steele (1999). The parameters consist of the geometric details and the elastic moduli of the components, about 70 in all.

2. Most components are orthotropic, i.e., have small to zero stiffness in the direction perpendicular to the cross-section. These are hair cells, cilia, pillar cells, and BM fiber layers. In a change from Steele (1999), the recticular laminar (RL), which is the membrane in which the tops of the IHC and OHC are embedded, and the pillar head are now also considered to be orthotropic.
3. Isotropic components are the tectorial membrane (TM), the BM ground substance, and the Hensen cells.
4. All tissue in the cochlear cross-section is linearly elastic.

Generally, the elastic moduli in Steele (1999) are consistent with the microstructure and the fairly well known measurements of OHC stiffness, volume compliance, and point loads in the GP. The significant modification is from the measurements of Tolomeo and Holley (1997) for the bending stiffness of pillar cells. The interior of these cells contains evenly spaced microtubules with cross-linking. When the cross-linking is removed, the increase in bending stiffness is only a factor of four. Since there are some 40 layers of microtubules for one plane of bending, strong cross-linking would give an increase of a factor of 1600. Therefore, the actual increase of four indicates that the effective transverse shear modulus of the cross-linking is rather low, around 300 Pa, compared to the longitudinal stiffness of the filaments of the microtubules of 2 GPa. Thus the pillar cells, as well as the Dieter rods, seem to be designed to have high longitudinal stiffness, but little bending stiffness. In addition, Tolomeo (personal communication) indicates the heads of the pillars can separate fairly easily, which corresponds to a small stiffness in the direction perpendicular to the cross-section.

This is relevant when considering the measurements of Ulfendahl et al. (2002), and Fridberger et al. (2002), which provide quantitative radial and axial components of displacement at various points in the OC cross-section of the GP upper turn for quasi-static pressure loading. Notable is that the displacements for pressure toward ST are substantially larger than those for pressure toward SV. From the calculations of the model (Fig. 1), it appears that this may be explained by mechanical buckling of the pillars. For pressure towards ST, the IP is in compression. Since this is not the focus of the present study, we merely summarize by saying that the elastic model is reasonably consistent with the measurements of Ulfendahl et al. (2002) when the low shear modulus of Tolomeo and Holley (1997) is used for the pillar cells and Deiter rods. The stiffness of OHC is from Spector et al. (1999). It appears that the model is also consistent with the measurements of RL motion by Hemmert et al. (2000), and Khanna et al. (1989).

Hornera et al. (2004) point out that a simple beam model for the BM can simulate the shape of the displacement observed by Cooper in the GP at all frequencies. The beam is loaded by uniform pressure and consists of different thicknesses in the pectinate and arcuate zones of the BM. For their beam, the left edge (at the primary spiral osseous lamina) is simply supported (i.e., hinged), and the right edge (at the spiral ligament) is clamped. Fig. 4 shows that our result, from the considerably more elaborate model of the cross-section at the base (Fig. 2) for the BM displacement under static pressure, compares well with Cooper's profile. For our calculation, both edges are clamped. We agree with Hornera et al. (2004) that the clamping on the right edge is important for GP.

The more elaborate model also agrees fairly well with point load measurements, for which the orthotropy of the structure is important. From our experience, it seems that a simple beam model cannot simulate both the Cooper profile with uniform pressure and the point load measurements in the GP. The actual orthotropic structure of the pillars must be considered.

There is always the question whether or not stiffness values from static tests are valid for the acoustic frequencies. Therefore the measurements of Scherer and Gummer (2004) are of considerable interest since the point impedance is measured for frequencies in the range 0.5–40 kHz. Points across the RL were measured in a GP preparation at different distances from the stapes. The BM was constrained and the TM removed, so just the properties of the OC are obtained. They used a curve fit with various viscoelastic parameters, one of which can be identified as the static point load stiffness. A comparison with the elastic model with BM constrained and TM removed is in Fig. 5. This calculation is preliminary, for

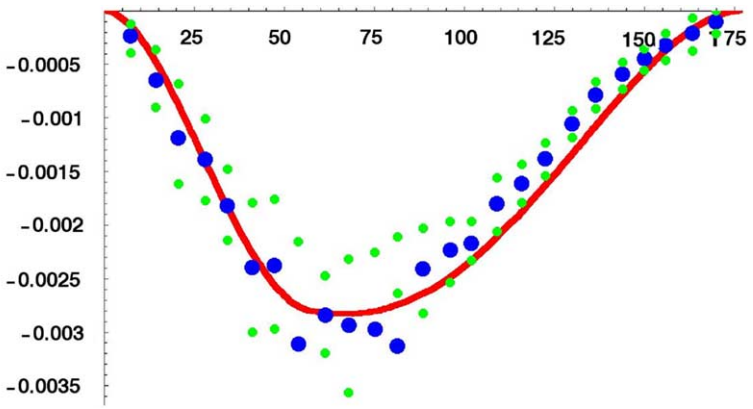

Fig. 4. Comparison of shape of BM displacement at the base. The solid curve is calculated at the base for pressure loading, and the big dots give the general shape measured by Cooper (Hornera et al., 2004). The small dots give their upper and lower bounds. The radial distance and calculated displacement for static pressure of 1 Pa are in microns.

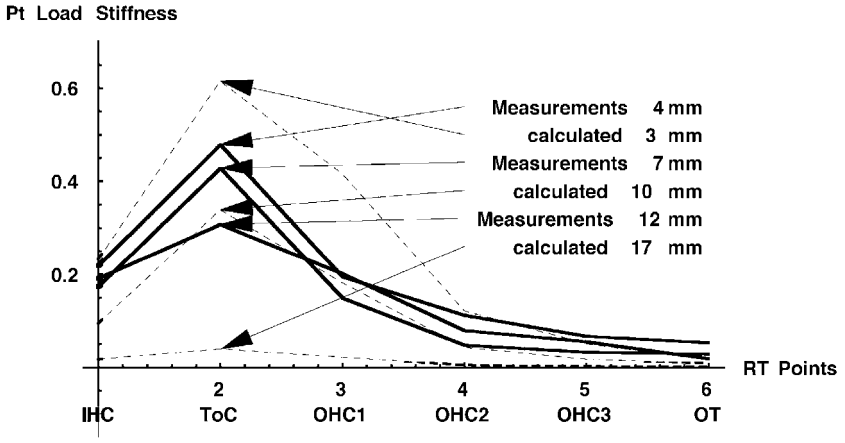

Fig. 5. Comparison of point load stiffness (N/m) at points across the RL for different distances from the stapes. The measurements are the static stiffness components of the curve fits of the impedance curves in Scherer and Gummer (2004). The calculated values are from the elastic model.

an axisymmetric line load with the point load presumed to act on a section 8 μm wide, corresponding to the pillar width. However, the general agreement indicates that the linearly elastic model is valid for acoustic frequencies and that the OC structure simulation is reasonable.

2.3. Equations for elastic behavior

In Steele (1999) a table of properties for each cochlear cross-section is the beginning. This is extended to include the IHC. A special computer program reads the table and generates the input file for Fast4 for each cross-section. The bookkeeping detail and the extensive validation will not be given here. However, the new feature is that the tip of the tallest cilium is near both the HS and the TM (Fig. 3). Therefore the forces acting on the opposing surfaces must be taken into account. In summary, the system vectors of force and displacement quantities consists of:

$$\mathbf{F} = \begin{bmatrix} p_{\mathrm{SV}} \\ p_{\mathrm{IS}} \\ p_{\mathrm{C}} \\ p_{L_1} \\ p_{L_2} \\ p_{L_3} \\ rq_{\mathrm{HS}} \\ rq_{\mathrm{TM}} \\ s_{L_1} \\ s_{L_2} \\ s_{L_3} \\ s_{L_4} \end{bmatrix}, \quad \mathbf{D} = \begin{bmatrix} rA_{\mathrm{SV}} \\ rA_{\mathrm{IS}} \\ rA_{\mathrm{C}} \\ rA_{L_1} \\ rA_{L_2} \\ rA_{L_3} \\ g_{\mathrm{HS}} \\ g_{\mathrm{TM}} \\ r\gamma_{L_1} \\ r\gamma_{L_2} \\ r\gamma_{L_3} \\ r\gamma_{L_4} \end{bmatrix}, \tag{1}$$

for a total of $N = 12$ elements. The fluid regions under the TM between the cilia of the hair cells are designated by $L_1, \ldots, L_4$. The p's are the pressures in the six fluid regions, and the A's are the area displacement. The pressure in ST is the reference pressure, taken to be zero. The q's are the opposing forces on the tips of the IHC cilium, and the g's are the gap displacements. The s's are the opposing shear forces on the surfaces of the regions $L_1, \ldots, L_4$ and the γ's are the corresponding shear strains multiplied by the cross-sectional area. The possible mechanical valve effect of the outer margin of the TM is not taken into account, so in the present model there is an independent fluid shear in L_4 given by s_{L_4}, but the pressure in L_4 is equal to p_{SV}. Because of the axisymmetric geometry, the force resultants are multiplied by the radius r, and the area and shear displacements are multiplied by r. Then the product $\mathbf{F} * \mathbf{D}/2$ is the work.

Fast4 generates the static elastic response for a unit value of each element of $\mathbf{F}$, which provides a column of the $N \times N$ symmetric elastic flexibility matrix for the structure $\mathbf{E}$:

$$\mathbf{D} = \mathbf{E}\mathbf{F}. \tag{2}$$

The calculation is efficient, requiring a few minutes on a laptop computer.

However, the fluid in region C (Fig. 1) is not connected to the fluid of the other regions. Since the fluid is incompressible, the change in area of this region, given by the element A_{C} in $\mathbf{D}$ must be zero. In addition, the pressure in SV is considered as prescribed, so the area displacement A_{SV} can be eliminated. After the standard manipulation, the equation becomes a modified version of Eq. (2):

$$\mathbf{D}_{\mathrm{red}} = \mathbf{E}_{\mathrm{red}}\mathbf{F}_{\mathrm{red}} + \mathbf{L}_{\mathrm{E}} p_{\mathrm{SV}}. \tag{3}$$

In which $\mathbf{L}_{\mathrm{E}}$ is the reduced first column of $\mathbf{E}$, and the reduced force and displacement vectors are:

$$\mathbf{F}_{\mathrm{red}} = \begin{bmatrix} p_{\mathrm{IS}} \\ p_{L_1} \\ p_{L_2} \\ p_{L_3} \\ rq_{\mathrm{HS}} \\ rq_{\mathrm{TM}} \\ s_{L_1} \\ s_{L_2} \\ s_{L_3} \\ s_{L_4} \end{bmatrix}, \quad \mathbf{D}_{\mathrm{red}} = \begin{bmatrix} rA_{\mathrm{IS}} \\ rA_{L_1} \\ rA_{L_2} \\ rA_{L_3} \\ g_{\mathrm{HS}} \\ g_{\mathrm{TM}} \\ r\gamma_{L_1} \\ r\gamma_{L_2} \\ r\gamma_{L_3} \\ r\gamma_{L_4} \end{bmatrix}. \tag{4}$$

The compliance matrix $\mathbf{E}_{\mathrm{red}}$ is symmetric and nonsingular.

2.4. Fluid

The present attention is on the constricted fluid region of the IHC cilia and between the RL and TM, the regions L_1, L_2, L_3, and L_4. The assumptions for the fluid are the following.

1. The displacement of fluid within the OC in the direction perpendicular to the cross-section is negligible for the long wavelengths at low frequencies. The fluid motion in the ST and SV causes a pressure difference acting on the OC, so we take p_{SV} as prescribed and $p_{ST} = 0$.
2. The flow of fluid between the IHC ciliary tips and the HS and TM is calculated with local Poiseuille flow. This is valid when the gap is small in comparison with the radius of the tip. No flow passing through the IHC cilia is considered.
3. The permeability of fluid around the ciliary bundles of the OHC's is based on experimental model measurements (Frommer and Steele, 1979).
4. The viscous shear resistance of the regions L_1, L_2, L_3, and L_4 is included.
5. The fluid has the viscosity of saline at body temperature.
6. Reissner's membrane is ignored, so there is only one fluid region SV above the OC.
7. The resistance of flow of Cortilymph (C) through the OP and OHC is ignored. Thus the condition on C is only that the area be preserved.
8. Fluid inertia is neglected for the low frequencies considered.

2.5. Equations for Poiseuille flow—Simple cilium contact model

A simple model (Fig. 6) shows the qualitative nature of the possible effect of the proximity of the tip of the IHC cilia and the HS. The displacement of the base u represents the relative displacement between the RL and the TM, and the HS is taken to be parallel to the axis of the cilium, which is an exaggeration. The flow of fluid between a flat surface and a cylindrical surface with the radius R can be approximated by plane

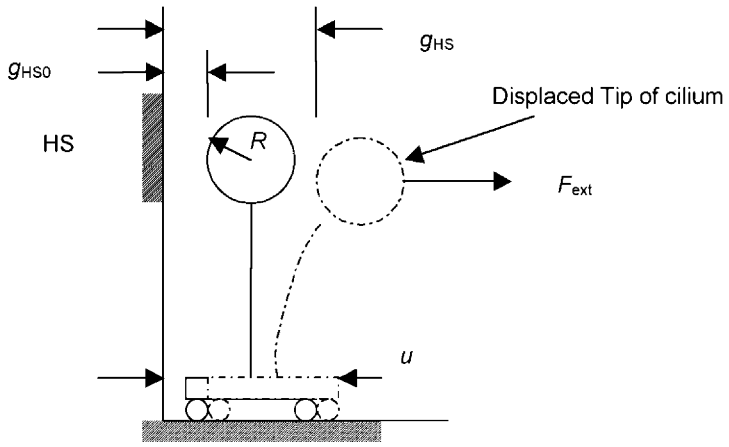

Fig. 6. Simple model for near contact of cilium and HS. The gap between the cilium and HS is g_{HS}, with the initial resting value g_{HS0}, the external force on the cilium acting away from HS is F_{ext}, the displacement of the base of the cilium is u, and the radius of the tip of the cilium is R. When the gap is small, the significant fluid effect is concentrated in the gap region.

Poiseuille flow (Lagerstrom and Chang, 1962), which provides the relation between pressure gradient and flow rate:

$$\frac{\mathrm{d}p}{\mathrm{d}x} = -\frac{12\mu}{H^3}\dot{Q}(x). \tag{5}$$

The pressure is p, the distance along the interface from the point of nearest contact is x, the viscosity of the fluid is μ, the area displacement of the fluid is Q, the dot indicates the time derivative, and the distance between flat and curved surface is the quadratic H:

$$H(x) = g_{\mathrm{HS}}(1 + \lambda x^2), \tag{6}$$

in which g_{HS} is the gap at the point of nearest contact, and the parameter λ is:

$$\lambda = \frac{1}{2Rg_{\mathrm{HS}}}. \tag{7}$$

For a velocity of opening of the gap, the flow is:

$$\dot{Q}(x) = \dot{g}_{\mathrm{HS}}x. \tag{8}$$

So integrating Eq. (5) yields the pressure distribution:

$$p(x) = -\frac{3\mu\dot{g}_{\mathrm{HS}}}{\alpha g_{\mathrm{HS}}^3(1 + \lambda x^2)^2}, \tag{9}$$

which shows that the pressure decreases rapidly with the distance x from the point of closest contact. Therefore this may be integrated to obtain the total force from the fluid resisting the motion:

$$F_{\mathrm{fluid}} = \int_{-\infty}^{\infty} p(x)\,\mathrm{d}x = -3\sqrt{2}\pi\mu\dot{g}_{\mathrm{HS}}\left(\frac{R}{g_{\mathrm{HS}}}\right)^{3/2}. \tag{10}$$

The spring stiffness of the cilium is assumed to be linear, so the equilibrium equation is:

$$K(g_{\mathrm{HS}} - u + b + R) = F_{\mathrm{ext}} + F_{\mathrm{fluid}}, \tag{11}$$

where b is the half width of the base, which yields the nonlinear differential equation:

$$\frac{1}{(1+\xi)^{3/2}}\frac{\mathrm{d}\xi}{\mathrm{d}\tau} + \xi = \xi_u + \xi_{\mathrm{ext}}, \tag{12}$$

in which the dimensionless quantities are defined by:

$$\begin{aligned}
&\xi = (g_{\mathrm{HS}} - g_{\mathrm{HS0}})/g_{\mathrm{HS0}},\\
&\xi_u = (u - g_{\mathrm{HS0}} - b - R)/g_{\mathrm{HS0}},\\
&\xi_{\mathrm{ext}} = F_{\mathrm{ext}}/(Kg_{\mathrm{HS0}}),\\
&\tau = t/T,\\
&T = \frac{3\sqrt{2}\pi\mu}{K}\left(\frac{R}{g_{\mathrm{HS0}}}\right)^{3/2},
\end{aligned} \tag{13}$$

in which τ is the time divided by the decay time T. Eq. (12) has reasonable behavior with the fluid resistance to motion becoming large as the gap becomes small for ξ approaching -1 and becoming small as ξ becomes large. The equation is most accurate for small gaps when the fluid is most significant. The dimensionless force of excitation, i.e., the net force bending the cilium is the response $\Phi = \xi - \xi_u$.

2.6. Permeability coefficients

For the full OC model (Fig. 1), fluid provides the relation between the force quantities and the flow rates:

$$\frac{\mathrm{d}\mathbf{D}_{\mathrm{red}}}{\mathrm{d}t} = -\mathbf{C}\mathbf{F}_{\mathrm{red}} + p_{\mathrm{SV}}\mathbf{L}_{\mathrm{C}}, \tag{14}$$

in which $\mathbf{C}$ is the permeability matrix, and $\mathbf{L}_{\mathrm{C}}$ is considered a load vector that is written separately because p_{SV} is prescribed. The elasticity matrix $\mathbf{E}_{\mathrm{red}}$ (Eq. (3)) is computed numerically and is full, reflecting the strong elastic coupling of all the regions. In contrast, the permeability matrix $\mathbf{C}$ is nearly diagonal, since the fluid in one region can flow to at most two neighboring regions, and only the fourth element of $\mathbf{L}_{\mathrm{C}}$ is nonzero. Thus the nonzero coefficients are:

$$\mathbf{C} = \begin{bmatrix} c_0 & -c_0 & & & & & & & \\ -c_0 & c_0 + c_1 & -c_1 & & & & & & \\ & -c_1 & c_1 + c_2 & -c_2 & & & & & \\ & & -c_2 & c_2 + c_3 & & & & & \\ & & & & c_{\mathrm{HS}} & & & & \\ & & & & & c_{\mathrm{TM}} & & & \\ & & & & & & c_{\mathrm{S}} & & \\ & & & & & & & c_{\mathrm{S}} & \\ & & & & & & & & c_{\mathrm{S}} \\ & & & & & & & & & c_{\mathrm{S}} \end{bmatrix}, \quad \mathbf{L}_{\mathrm{C}} = \begin{bmatrix} \\ \\ \\ c_3 \\ \\ \\ \\ \\ \\ \end{bmatrix}. \tag{15}$$

For small gaps, the significant fluid response is localized to the regions of the nearest contact, as shown in Fig. 7. Thus two coefficients are from the reciprocal of Eq. (9):

$$c_{\mathrm{HS}} = \frac{1}{3\sqrt{2}\pi\mu r}\left(\frac{g_{\mathrm{HS}}}{R}\right)^{3/2}, \quad c_{\mathrm{TM}} = \frac{1}{3\sqrt{2}\pi\mu r}\left(\frac{g_{\mathrm{TM}}}{R}\right)^{3/2}. \tag{16}$$

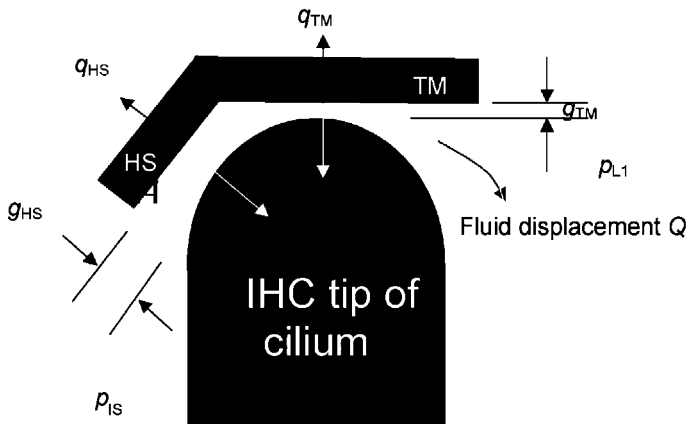

Fig. 7. Very close view of tip of tallest cilium for OC model. The HS and TM are considered to be two straight surfaces and the tip of the cilium as a semicircle with radius R. The fluid gap between the tip and the HS is g_{HS} and that between the tip and the TM is g_{TM}. The force due to the fluid is localized to the region of nearest contact and has the resultants q_{HS} and q_{TM}, which act on the opposing surfaces.

The coefficients c_S describe the fluid shear in the regions L_1, L_2, L_3, and L_4:

$$c_S = \frac{r * \text{Height of cilia} * \text{Length of region}}{\mu}. \tag{17}$$

The flow between a flat and a cylindrical surface can also be approximated by Poiseuille flow Eq. (5), with $\dot{Q}$ constant. Integrating yields the pressure drop:

$$-\Delta p = \frac{9\pi\mu}{g^2}\left(\frac{R}{2g}\right)^{1/2}\dot{Q}, \tag{18}$$

where R is the radius and g is the gap width. For the tip of the IHC cilium, there are two gap regions (Fig. 7), which provide impedance in series. Therefore the total permeability coefficient is:

$$c_0 = \frac{r\sqrt{2}g_{TM}^{5/2}}{9\pi\mu\sqrt{R}}\frac{1}{1+(g_{TM}/g_{HS})^{5/2}}. \tag{19}$$

A similar result is used for the permeability of flow around the bundles of the OHC:

$$c_1 = \frac{r\sqrt{2}g_{\text{effective}}^{5/2}}{9\pi\mu\sqrt{R}}\left(\frac{\text{Length of cilium}}{\text{Diameter of OHC}}\right). \tag{20}$$

The tallest OHC cilium is attached to the TM, so the flow is through the gap between the ciliary bundles. Fortunately, the flow in a large scale experimental model of the ciliary bundles has been measured (Frommer and Steele, 1979). The coefficient Eq. (20) agrees with the measurements if the effective gap is taken to be:

$$g_{\text{effective}} \approx \frac{\text{Diameter of OHC}}{10}. \tag{21}$$

2.7. Equations for coupling structure and fluid

The elastic forces from Eq. (3) and fluid forces from Eq. (14) must be the same. Equating these yields the first order system of equations:

$$\mathbf{F}_{red} = -\mathbf{C}^{-1}\left(\frac{d\mathbf{D}_{red}}{dt} - p_{SV}\mathbf{L}_C\right) = \mathbf{E}_{red}^{-1}(\mathbf{D}_{red} - p_{SV}\mathbf{L}_E), \tag{22}$$

which can be rewritten as:

$$\mathbf{G}\frac{d\mathbf{D}_{red}}{dt} + \mathbf{D}_{red} = p_{SV}(\mathbf{L}_E + \mathbf{G}\mathbf{L}_C), \tag{23}$$

where $\mathbf{G} = \mathbf{E}_{red}\mathbf{C}^{-1}$ is a matrix whose eigenvalues are decay times for the complementary solutions. For when the displacement is small in comparison with the initial gap, the matrix $\mathbf{G}$ and the right hand side are constant, so the linear solution is readily computed. For the generalization of the simple model Eq. (12) to the full OC model, the coefficients in Eqs. (16), (19), and (20) must have the current gap size, rather than the initial. This makes the matrix $\mathbf{G}$ and the right-hand-side of Eq. (23) nonlinear functions of the elements of $\mathbf{D}$.

3. Results

First the near contact behavior of a cilium tip and a surface is demonstrated with the simple model (Fig. 4). Forward integration of Eq. (12) readily converges to a steady-state solution, so the present results for the

nonlinear response can be easily verified. The equations for the full model of the OC are substantially more involved, but the results appear to be "reasonable". At this time only the results for the linear behavior of the full model are available.

3.1. Simple model

The input we consider is a sinusoidal variation in the external force on the cilia, due to a pressure difference between the fluid regions IS and L_1 (Fig. 1), represented by ξ_{ext} and a relative displacement between the HS and the TM, represented by ξ_u:

$$\begin{aligned} \xi_{\text{ext}} &= \varepsilon\alpha\cos(\omega\tau), \\ \xi_u &= \varepsilon\beta\cos(\omega\tau). \end{aligned} \tag{24}$$

Forward integration of Eq. (12) for $\alpha = 1$ and $\beta = 0.2$ with the initial condition $\xi(0) = 0$ yields the results shown in Fig. 8 for various values of driving frequency ω (columns) and amplitude ε (rows). The transients decay rapidly, within a cycle of input. For small amplitude of input, the response Φ is also sinusoidal and in phase with the input for low frequency. As the amplitude of the input ε increases in magnitude, the response Φ becomes quite nonlinear, with a sharp spike that is more pronounced for the lower frequency. Direct

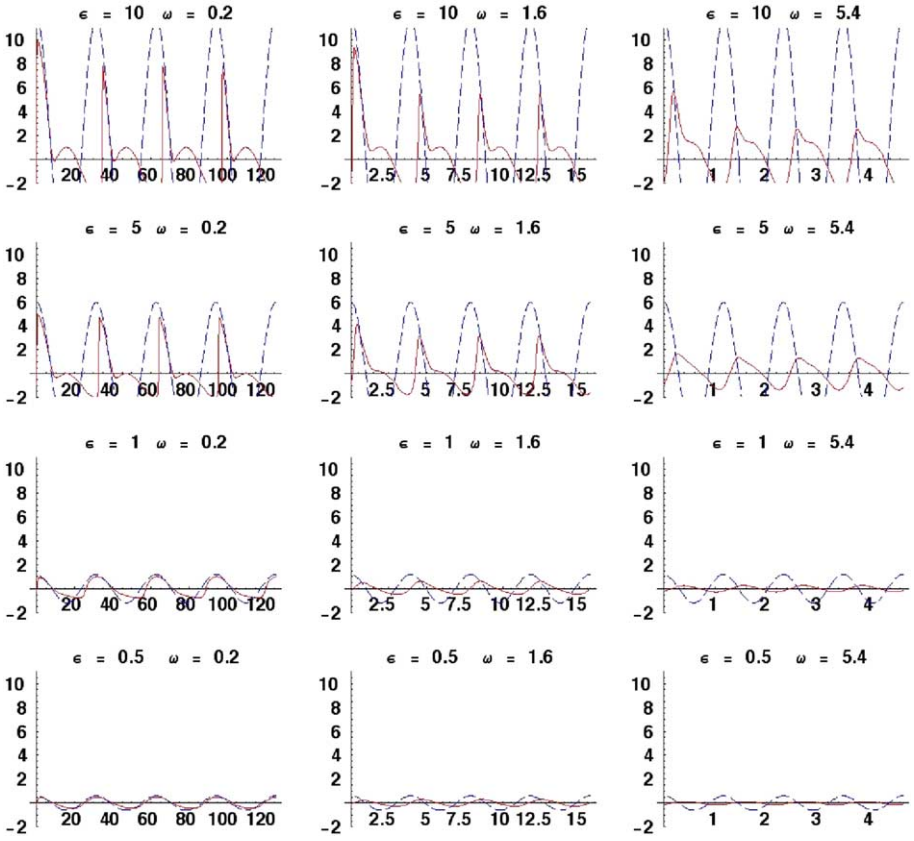

Fig. 8. Nonlinear response of simplified hair cell model. The dimensionless parameters are the amplitude of input ε and the frequency ω. The horizontal scale is the time. The solid curve shows the excitation force on the cilium and the dashed curve shows the input, which is a combination of force F_{ext} and base displacement g, given by the parameters $\alpha = 1$ and $\beta = 0.2$.

measurements of the response of inner hair cells (Mountain and Cody, 1999) in Fig. 9 show rather similar behavior. The voltage in the scala media on the left shows the sinusoidal pattern with the well-known saturation of the intracellular potential, that mainly squares the sinusoid. The pattern of IHC responses on the right is clearly different and quite similar to the response of the simple model (Fig. 8). Notice that for a

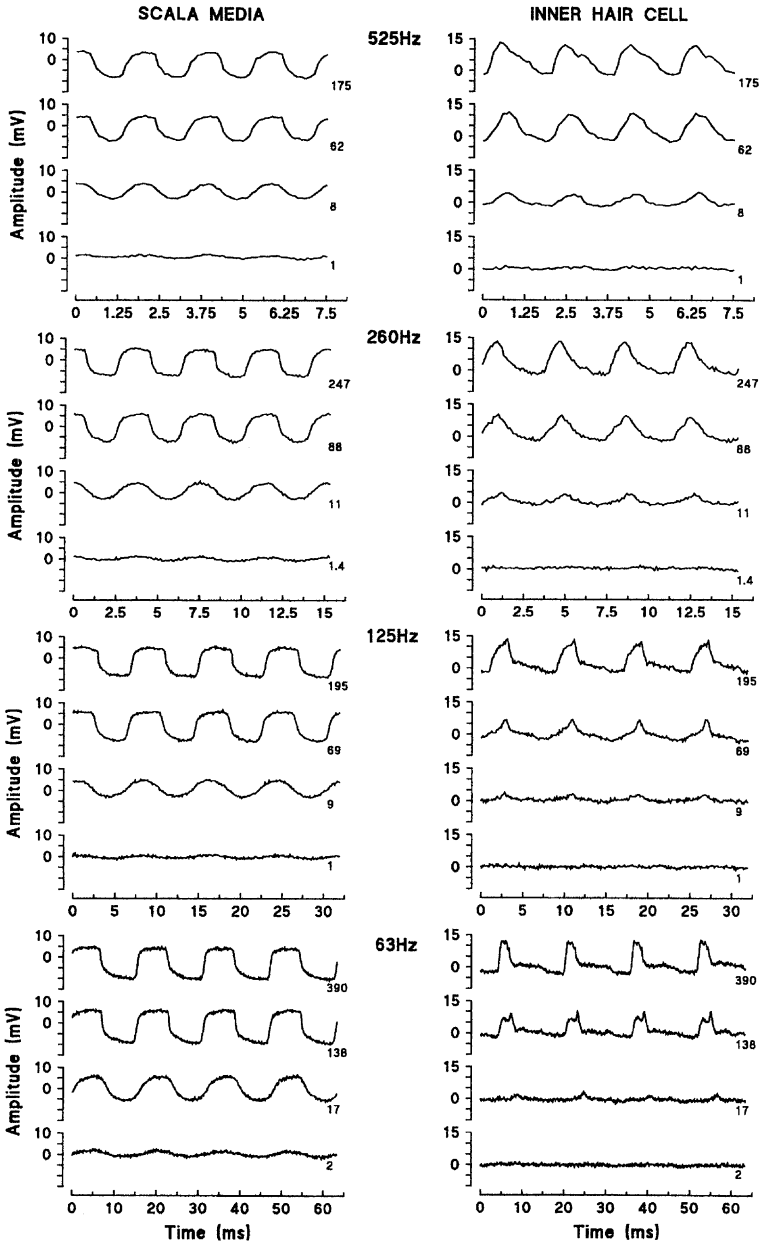

Fig. 9. Measurements from Mountain and Cody (1999). On the left are voltages recorded in the surrounding fluid (scala media), which is presumed to reflect the activity of the outer hair cells. On the right are voltages recorded intracellularly from an IHC. The numbers on each response curve is an approximation for the amplitude of the BM vibration.

given frequency, the peak sharpens with amplitude, while the peak sharpens with decreasing frequency for a given amplitude. Not shown is that a saturation model for the IHC transduction smoothes the curves but does not change the basic behavior.

This appears to be an indication that the near contact of the IHC cilia with the HS (Edge et al., 1998) is an important feature of IHC excitation in the mammalian cochlea. Therefore, the more accurate model for the OC using the near contact of cilium tip and HS is warranted.

3.2. Full model

For sufficiently small displacements, the coefficients in the matrices and vectors are constant, so Eq. (23) is linear. The steady-state solution is:

$$p_{\mathrm{SV}} = P\mathrm{e}^{\mathrm{i}\varpi t}, \quad \mathbf{D}_{\mathrm{red}} = \mathbf{H}\mathrm{e}^{\mathrm{i}\varpi t}, \quad \mathbf{H} = P(\mathbf{G}\mathrm{i}\varpi + \mathbf{I})^{-1}(\mathbf{L}_{\mathrm{E}} + \mathbf{G}\mathbf{L}_{\mathrm{C}}), \tag{25}$$

which is easily computed for various frequencies of excitation. After the elastic flexibility matrix is computed, the solution of Eq. (25) is fast, so a number of cases of frequency and gap spacing can be analysed in a second of computing time.

After the solution Eq. (25) is computed, the force in the tip link is calculated. The force is divided by the height of the cilium for the effective pressure acting on the tip links, with respect to p_{SV}. The amplitude of the effective pressure for the GP upper turn depends significantly on the initial gap between the cilium tip and HS and TM (Fig. 10). Because of the restriction of the present model, only the frequencies less than 400 Hz are shown. A two-digit number labels the curves. The first number is ratio g_{HS}/R, the gap between the cilium and HS divided by the tip radius, expressed as percentage. The second number is the percentage of g_{TM}/R. The curves for 1% HS gap (11, 14, 17) are about the same, which indicates that the amplitude is insensitive to the magnitude of the gap with TM. In contrast, the loading of the tip fiber is substantially reduced when the HS gap is increased to 4% and 7%, even when the gap to TM is small (41, 71, 44, 77). The phase (Fig. 11) also shows sensitivity to the HS gap but not much to the TM gap. The phase for low frequency is around 90°, which indicates maximum IHC excitation for BM velocity towards SV. For higher frequency the phase decreases toward zero, which would correspond to maximum excitation for BM displacement toward SV. The IHC and auditory nerve fiber recordings for the GP upper turn (Cheatham and Dallos, 1999), stay near 90° to about 400 Hz before decreasing. So the present model is

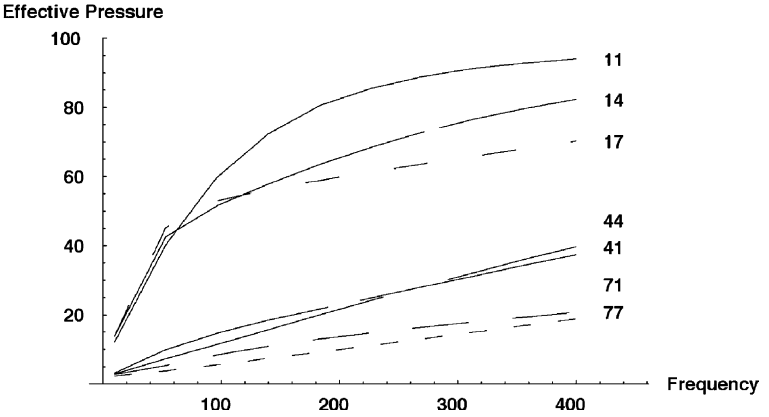

Fig. 10. Amplitude of tension in the tip link of the IHC cilia as a function of frequency at the apex for soft TM. The tension is normalized to an effective pressure, on a linear scale. Various values of the gaps are designated by the two digit labels. The first and second digits indicate the gaps with HS and TM, respectively, expressed as a percentage of the cilium tip radius.

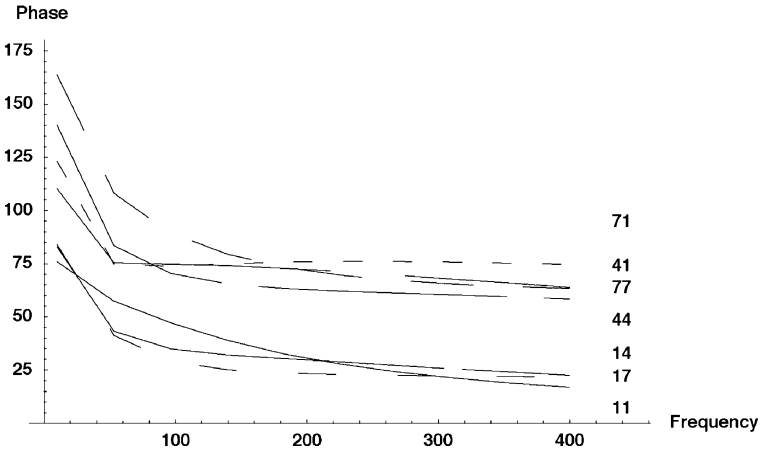

Fig. 11. Phase (in degrees) of tension in the tip link of the IHC cilia as a function of frequency at the apex for soft TM. If the maximum tip link tension occurs when the BM displacement is at the maximum excursion toward scala vestibuli, the phase is zero. If the maximum tension occurs when the BM velocity is at the maximum toward scala vestibuli, the phase is equal to 90°. The calculations are for various values of the gaps as designated by the two digit labels, as before. The lines labeled 11, 14, and 17 show that for a small gap with Hensen's stripe, the result is insensitive to the gap to the TM. The phase is between 0° and 90°.

quantitatively deficient, but provides the qualitative correct tendency. As suggested (Cheatham and Dallos, 1999), the phase depends on the viscoelastic behavior of the fluid and tissue. For lower frequency, the IHC cilia are dragged through the fluid, and respond for velocity toward SV. For higher frequency, the fluid in the gap between cilia and HS resists motion, so the cilia are more "stuck" to the HS, and the excitation occurs for displacement toward SV.

Quite contradictory results are found in the basal turn (Cheatham and Dallos, 1999) and (Ruggero et al., 2000). The auditory nerve fibers respond to BM velocity toward ST, while the IHC recordings are similar to those in the apex. A variety of possible causes are suggested by several authors and summarized by Cheatham and Dallos (1999) and Ruggero et al. (2000). Two of these can be explored with the present model. First is the effect of the different geometry in the base (Fig. 2), and second is the effect of mechanical constraint caused by the insertion of a microelectrode into the IHC. The "electrode" in Fig. 12 simulates entry through ST. The electrode is modeled as solid glass, and so is essentially rigid in comparison to the tissue of the OC, so the point of penetration of the BM and the IHC are essentially fixed. Since the present calculation ignores variation of tissue or fluid out of the plane, the "electrode" is a sheet, and therefore should provide more constraint than an actual 3-D probe. Also computations have been made (Steele and Puria, 2003) with the electrode entering the OC parallel to the BM, as used by Cheatham and Dallos (1999).

The results for the simulation of both types of electrodes show no qualitative deviation from the phase in Fig. 11. However, the amplitude of the excitation in Fig. 10 is substantially reduced by the constraint in Fig. 12. Substantial changes in the values used for the permeability of the flow through the OHC cilia and past the IHC cilium have little effect on the phase.

Various possibilities for reasonable modifications of the elastic and fluid properties have been considered. The one found to have a substantial effect is the stiffness of the TM. Fig. 13 shows the results for the cross-section at the base with the Young's modulus of the TM ranging over several orders of magnitude, with all other parameters kept constant. Thus high stiffness causes the phase to be well over 180°. The TM is the most difficult tissue in the OC to quantify. Abnet and Freeman (2000) measure the deformation due to a tangential point load on the excised mouse TM. The stiffness for radial load ranges from 0.07 to 1 N/m, with an average of 0.18 N/m. A careful computation with a simulation of the experimental situation would

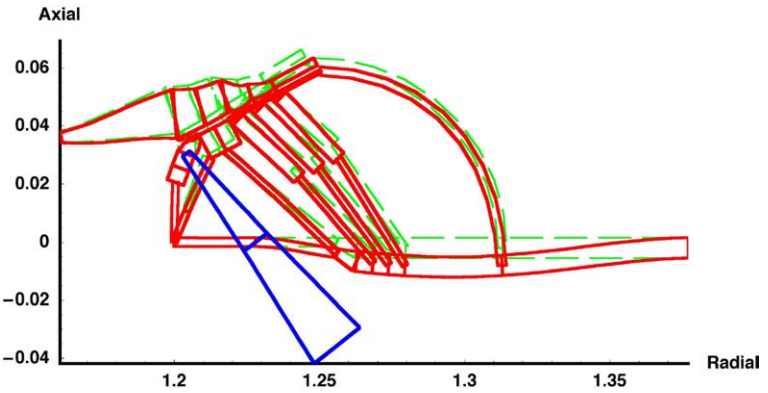

Fig. 12. Probe from ST at base. The probe is assumed to stick to the center of the arcuate zone of the BM and the IHC, so the displacement is constrained at these points. The constraint greatly reduces the effective pressure on the IHC tip link, but does not have much effect on the phase.

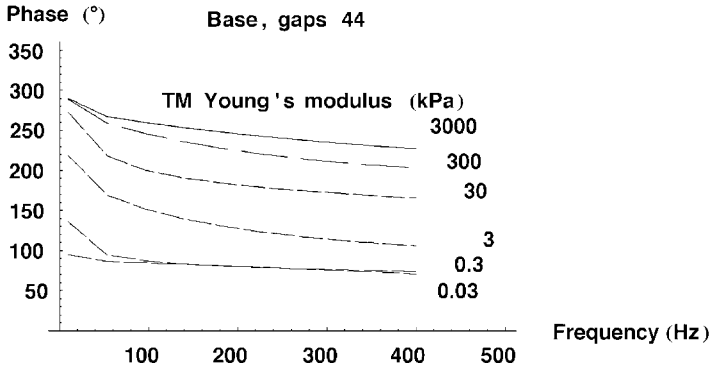

Fig. 13. Phase of effective pressure on IHC cilia at the base. For this calculation the stiffness of the OC is reasonable, and the initial gaps with the HS and TM are both equal to 4%. The Young's modulus of the TM is set to the reasonable value of 30 kPa, and values orders of magnitude stiffer and softer. The reasonable value gives a phase similar to the neural recordings in the base of the chinchilla (Ruggero et al., 2000), with the excitation occurring for velocity toward ST (270°) for low frequency and approaching displacement toward ST (180°) for higher frequency.

be required to interpret the point load stiffness as a tissue Young's modulus E. However, our rough approximation is that the point load stiffness of 0.18 N/m corresponds to $E = 30$ kPa, which in Fig. 13 gives a phase near 180°, i.e., excitation for BM displacement toward ST. Higher values of E are certainly possible, considering the roughness of our interpretation and the range of values for the point load stiffness. An increase to 300 kPa, which is still a rather soft material, moves the phase closer to 270°, i.e., excitation for BM velocity toward ST.

For the base, the displacement of the BM for the higher TM stiffness still is similar to that shown in Fig. 4, i.e., in agreement with Cooper's profile. For the apex, however, that is not the case. To obtain the agreement in Fig. 4 and agreement with the motion of the OC measured by Fridberger et al. (2002), the TM must be soft, around 0.3 kPa.

The usual thought is that the BM velocity toward ST will cause the IHC cilia to be pulled through the fluid, which will bend the tips of the cilia inward, in the inhibitory direction. However, another effect can be seen in Figs. 1 and 2. For static pressure on the BM toward ST, the area of region L_1 increases. When all is filled with fluid, then fluid is pulled from IS to L_1. This causes an outward bending of the cilia, i.e.,

excitation. For the softer TM, the portion over the IS just accommodates, and the pressure in IS and L_1 is nearly the same. So the relation of the IHC cilia to the HS dominates. However, when the TM is stiff, the portion of the TM over the IS does not accommodate, the pressure in L_1 is lower than in IS, typically around 5%, which dominates the stress in the tip link.

4. Conclusion

The present effort to simulate the fluid flow between the RL and TM and around the IHC cilia is a step toward more accurate and informative models of the cochlear function.

The indication (Edge et al., 1998) that the IHC cilia are near the HS is important for the excitation of the IHC. The present simple, nonlinear, fluid-elastic model shows wave form dependence on amplitude and frequency that is similar to IHC electrical measurements (Mountain and Cody, 1999). This supports the inclusion of the near-contact model for IHC cilia into the elaborate elastic model for all the tissue of the OC.

The results for a soft TM with various gaps between the tip of the cilia of the IHC and the Hensen stripe and TM are what most would expect. The IHC excitation, which is calculated as maximum tension in the tip link, occurs roughly for BM velocity toward SV, with shift to BM displacement toward SV as frequency increases. With higher frequency the effect of the viscosity increases and the tip of the cilia will "stick" more to the Hensen stripe and the TM. The model indicates that this behavior is robust, i.e., it is not significantly modified by fairly substantial changes in the elastic and fluid properties. A simulation of the constraint due to an electrode penetrating the IHC also shows no significant change in the phase of excitation. So the simulation results are in qualitative agreement with the neural and IHC recordings made in the GP middle and upper turns and with the IHC recordings made in the base. Ruggero et al. (2000), however, find that the neural recordings in the base of the chinchilla have the excitation for BM velocity toward ST. The model has close to this behavior for a TM with a Young's modulus that appears to be consistent with the point load stiffness measured by Abnet and Freeman (2000). So all seems to fit with a TM that has a reduction in collagen fiber density of two orders of magnitude at the apex. This may not be unreasonable, since the BM and other components have a reduction of one order of magnitude.

The calculations certainly show that the excitation is not locked to a particular point of BM motion, but depends on the geometry, stiffness and fluid parameters.

The nonlinear solution for the complete model can also be carried out by forward integration, and will be a next step. In addition, the point is made (Cheatham and Dallos, 1999) that the length of the IHC cilia is greater than that of the OHC cilia in the base, which correlates with the phase of IHC excitation. For our present model, the height of both is taken to be the same. This could well affect the pressures in the $L_1, \ldots, L_4$ regions. There are other geometric details that should be improved. Not previously mentioned is that the model indicates that the shear force on the cilia of the first row of OHC is much larger than on the others for the soft TM. For the stiff TM in the upper turns, the maximum shear can occur in the cilia of the second row. Indeed, the shear on the first and second rows can be out-of-phase. One might expect that the shear on the three rows would be somewhat balanced and in-phase, which is another indication that the TM must be softer at the apex. The requirements are that stiffness be (1) consistent with the microstructure, (2) produce OC response consistent with the static point and pressure loads, and (3) deformation consistent with the details of the OC motion now available. This does not leave too much leeway in tuning the stiffness parameters. Much improvement remains to be achieved, but we have been moderately successful in satisfying these requirements with the present model.

Acknowledgment

A portion of this work was supported by Grant RGP0051 from the Human Frontier Science Program.

References

Andoh, M., Wada, H., 2003. Dynamic characteristics of the force generated by the outer hair cell motility in the organ of Corti—(Theoretical consideration). JSME Int. J. Ser. C—Mech. Syst. Mach. Elements Manufact. 46 (4), 1256–1265.

Abnet, C.C., Freeman, D.M., 2000. Deformations of the isolated mouse tectorial membrane produced by oscillatory forces. Hearing Res. 144, 29–46.

Bohnke, F., Arnold, W., 1998. Nonlinear mechanics of the organ of Corti caused by Deiters cells. IEEE Trans. Biomed. Eng. 45 (10), 1227–1233.

Cai, H., Chadwick, R., 2002. Radial structure of traveling waves in the inner ear. SIAM J. Appl. Math. 63 (4), 1105–1120.

Cheatham, M.A., Dallos, P., 1999. Response phase: A view from the inner hair cell. J. Acoust. Soc. Am. 105 (2 Pt 1), 799–810.

Dunnebier, E.A., Segenhout, J.M., Verheul, J., Albers, F.W.J., Dijk, G., Wit, H.P., 1998. Cochlear ultrastructure in two-phase endolymphatic hydrops in the guinea pig, University Library Groningen (Chapter 7).

Edge, R.M., Evans, B.N., Pearce, M., Richter, C.P., Hu, X., Dallos, P., 1998. Morphology of the unfixed cochlea. Hearing Res. 124 (1–2), 1–16.

Fridberger, A., Boutet de Monvel, J., Ulfendahl, M., 2002. Internal shearing within the hearing organ evoked by basilar membrane motion. J. Neurosci. 22 (22), 9850–9857.

Frommer, G., Steele, C.R., 1979. Permeability of fluid flow through hair cell cilia. J. Acoust. Soc. Am. 65, 659–764.

Givelberg, E., Bunn, J., 2003. A comprehensive three-dimensional model of the cochlea. J. Comput. Phys. 191 (2), 377–391.

Hornera, M., Champneys, A., Hunt, G., Cooper, N., 2004. Mathematical modeling of the radial profile of basilar membrane vibrations in the inner ear. J. Acoust. Soc. Am. 116 (2), 1025–1034.

Hemmert, W., Zenner, H.P., Gummer, A.W., 2000. Three-dimensional motion of the organ of Corti. Biophys. J. 78 (5), 2285–2297.

Kelly, J.P., 1989. Morphometry of the apical turn of the guinea pig's cochlea. Acta Otolaryngol. Suppl. 467, 113–122.

Khanna, S.M., Flock, A., Ulfendahl, M., 1989. Changes in cellular tuning along the radial axis of the cochlea. Acta Otolaryngol. Suppl. 467, 163–173.

Kolston, P.J., 1999. Comparing in vitro, in situ, and in vivo experimental data in a three-dimensional model of mammalian cochlear mechanics. Proc. Natl. Acad. Sci. 96 (7), 3676–3681.

Lagerstrom, P.A., Chang, I.D., 1962. Flow at low Reynolds numbers. In: Flugge, W. (Ed.), Handbook of Engineering Mechanics. McGraw-Hill, pp. 81-1–81-30.

Lim, K., Steele, C.R., 2003. Response suppression and transient behavior in a nonlinear active cochlear model with feed-forward. Int. J. Solids Struct. 40 (19), 5097–5107.

Mountain, D.C., Cody, A.R., 1999. Multiple modes of inner hair cell stimulation. Hear. Res. 132 (1–2), 1–14.

Narayan, S.S., Temchin, A.N., Recio, A., Ruggero, M.A., 1998. Frequency tuning of basilar membrane and auditory nerve fibers in the same cochleae. Science 282, 1882–1884.

Ruggero, M.A., Narayan, S.S., Temchin, A.N., Recio, A., 2000. Mechanical bases of frequency tuning and neural excitation at the base of the cochlea: Comparison of basilar-membrane vibrations and auditory-nerve-fiber responses in chinchilla. Proc. Natl. Acad. Sci. USA 97 (22), 11744–11750.

Scherer, M.P., Gummer, A.W., 2004. Impedance analysis of the organ of Corti with magnetically actuated probes. Biophys. J. 87 (2), 1378–1391.

Spector, A.A., Brownell, W.E., Popel, A.S., 1999. Estimation of elastic moduli and bending stiffness of the anisotropic outer hair cell wall. J. Acoust. Soc. Am. 103, 1007–1011.

Steele, C.R., 1999. Toward three-dimensional analysis of cochlear structure. ORL J. Otorhinolaryngol. Relat. Spec. 61 (5), 238–251.

Steele, C.R., Puria, S., 2003. Analysis of forces on inner hair cell cilia. In: Gummer, A.W. (Ed.), Biophysics of the Cochlea. World Scientific, pp. 359–367.

Steele, C.R., Shad, K.u.-R., 1995. Asymptotic-numeric solution for shells of revolution. Appl. Mech. Rev. 48 (11, part 2).

Steele, C.R., Taber, L.A., 1979. Comparison of WKB calculations and experimental results for three-dimensional cochlear models. J. Acoust. Soc. Am. 65 (4), 1007–1018.

Tolomeo, J.A., Holley, M.C., 1997. Mechanics of microtubule bundles in pillar cells from the inner ear. Biophys. J. 73, 2241–2247.

Ulfendahl, M., Boutet de Monvel, J., Le Calvez, S., 2002. Exploring the living cochlea using confocal microscopy. Audiol. Neurootol. 7 (1), 27–30.

Weinbaum, S., Guo, P., You, L.D., 2001. A new view of mechanotransduction and strain amplification in cells with microvilli and cell processes. Biorheology 31 (2–3), 119–142.

Zetes, D.E., Tolomeo, J.A., Holley, M.C., 2004. Mapping the mechanical properties of cytoskeletal structures in the mammalian inner ear, Unpublished manuscript.